Mechanics Research Communications 143 (2025) 104361

Contents lists available at ScienceDirect

Mechanics Research Communications

journal homepage: www.elsevier.com/locate/mechrescom

Transient torsional wave propagation in finite and infinite multilayered pipes

Chuanwen Chen [a,b], Yang Xiang [b,*], Lei Qin [a], Liguo Tang [c,d,e,*], Wenyu Luo [d,f]

[a] Beijing Key Laboratory for Sensors, Beijing Information Science & Technology University, Beijing 100192, China
[b] Fujian Provincial Key Laboratory of Light Propagation and Transformation, College of Information Science and Engineering, Huaqiao University, Xiamen 361021, China
[c] Shenzhen Research Institute of Xiamen University, Shenzhen 518000, China
[d] State Key Laboratory of Acoustics, Institute of Acoustics, Chinese Academy of Sciences, Beijing 100190, China
[e] Key Laboratory of Underwater Acoustic Communication and Marine Information Technology, College of Ocean and Earth Sciences, Xiamen University, Xiamen 361010, China
[f] University of Chinese Academy of Sciences, Beijing 100049, China

ARTICLE INFO

Keywords:
Multilayered pipes
Transient torsional waves
Eigenfunction expansion method
Nondestructive evaluation

ABSTRACT

Multilayered pipes are widely used in many engineering settings. Using guided wave is one of the most efficient techniques to inspect them. To inspect multilayered pipes using guided waves, it is of paramount importance to investigate the excitation and propagation of the guided wave within them. In this study, the solution of the elastodynamic response of the finite and infinite multilayered pipes to axisymmetric torsional body and surface forces is derived by the eigenfunction expansion method (EEM), based on which the excitation and propagation of each torsional mode can be quantitatively investigated. As an example of the application of the theory presented here, the transient torsional waves propagating in an Al-Cu bi-layered pipe is numerically studied. The numerically evaluated analytic solution agrees very well with that obtained using the finite element method (FEM).

1. Introduction

Multilayered pipes play an important role in many engineering settings [1–3]. For example, sandwich pipes are commonplace in deep subsea pipelines for oil and gas to meet demands for thermal insulation and mechanical integrity [4,5]. Coated pipes are commonplace in the petrochemical and aerospace industries [6]. There are numerous demands on nondestructive evaluation (NDE) to detect defects in multilayered pipes in service or production. The technique of guided waves for oil and gas pipeline inspection is very attractive due to its high efficiency and low cost [7–14]. There are numerous torsional, longitudinal and flexural modes propagating in pipes, which are designated by the symbols $T(0,m)$, $L(0,m)$ and $F(n, m)$ ($n, m = 1, 2, \ldots$), respectively [15–17].

To inspect multilayered pipes using guided waves, it is of paramount importance to investigate the excitation and propagation of transient guided torsional waves in the pipes. Karpfinger et al. [18] studied the Stoneley wave dispersion and attenuation propagation in cylindrical structures composed of fluid, elastic and poroelastic layers using the spectral method. Aguiar et al. [19] carried out the dynamic analysis of multilayered steel catenary risers using a novel, multilayered pipe beam element model. Banerjee and Kundu [20] studied the elastic wave field in multilayered nonplanar solid structures using a mesh-free semi-analytical approach. Predoi [21] studied the dispersion of guided waves in orthotropic multilayered pipes using a semi-analytical finite element (SAFE) algorithm. Barshinger and Rose [22] studied the free guided wave propagation in an elastic hollow cylinder coated with a viscoelastic material.

To reduce the difficulty caused by multimodes and dispersion, a single guided wave mode in a nondispersive region is often excited to inspect pipes [23,24]. In recent years, guided torsional wave for a single wall pipe inspection has received a lot of interest [25–31], as its propagation characteristics are not affected by the presence of liquid in the pipe. Moreover, it is easy to be excited and sensitive to circumferential defects.

Numerical techniques such as the finite element method (FEM) and

* Corresponding authors.
E-mail addresses: yxiang@hqu.edu.cn (Y. Xiang), liguotang@xmu.edu.cn (L. Tang).

https://doi.org/10.1016/j.mechrescom.2024.104361
Received 27 August 2024; Received in revised form 19 November 2024; Accepted 4 December 2024
Available online 9 December 2024

analytical techniques such as the eigenfunction expansion method (EEM) are often used to study the excitation and propagation of transient guided wave in pipes. The propagation of the transient wave in pipes within an arbitrary section, as well as the interaction between them and any defects can be simulated by the FEM. However, the transient excitation of each guided wave mode cannot be simulated by the FEM. The EEM cannot be used to study the interaction between guided waves and defects. However, it can study the excitation and propagation of each guided wave mode in a perfect pipe. The introduction of the EEM for solving elastodynamic problems can be found in Ref. [32–34]. Tang and his colleagues studied the transient torsional vibration responses of finite, semi-infinite and infinite hollow cylinders [32] and the transient wave propagation in liquid-filled pipe systems [34] using the EEM. Yin and Yue [35] investigated the transient plane-strain response of multilayered elastic cylinders to axisymmetric impulses using the EEM.

In this paper, the eigenfunctions corresponding to a finite multilayered pipe with traction-free lateral and end boundaries are obtained. The exact analytical transient torsional response of the finite multilayered pipe to external body forces is constructed using the EEM, based on which approximate analytical transient torsional response of the pipe to external surface forces is derived. Moreover, the analytical solution for transient torsional guided wave propagation in the finite multilayered pipe is extended explicitly and concisely to the infinite one. As an example of the application of the theory presented here, the transient torsional waves propagating in an Al-Cu bi-layered pipe is numerically studied. The numerically evaluated analytical solution agrees very well with that obtained using the FEM. The present solution can provide some theoretical guidelines for the guided wave NDE of multilayered pipes.

2. Statement of problem

A finite N-layered pipe of length $2L$, as shown in Fig. 1, is considered. We assume that each layer is an isotropic and homogeneous elastic body denoted by Ω_i ($i = 1, 2, 3, \ldots, N$). The inner and outer radius of the ith layer are denoted by r_{i-1} and r_i, respectively. The density and Lamé's second constant of the ith layer are ρ_i and μ_i, respectively. The inner and outer boundaries of the ith layer are denoted by Σ_{i-1} and Σ_i, respectively. The left and right boundaries of the ith layer are denoted by $\Sigma L\,i$and $\Sigma R\,i$, respectively. When the pipe is subjected to homogeneous, axisymmetric torsional loads $f(r, z, t)$, longitudinal and flexural waves cannot be excited. Its motion is governed by

$$\mathbf{L}_i\left[u_i^\theta(r,z,t)\right] + \rho_i f_i(r,z,t) = \rho_i \frac{\partial^2 u_i^\theta(r,z,t)}{\partial t^2} \text{ in } \Omega_i \ (i = 1,\ 2,\ \ldots,\ N) \tag{1}$$

where

$$\mathbf{L}_i = \mu_i\left(\frac{\partial^2}{\partial r^2} + \frac{1}{r}\frac{\partial}{\partial r} - \frac{1}{r^2} + \frac{\partial^2}{\partial z^2}\right), \tag{2}$$

We will determine the analytical solution to (1), which satisfies the initial conditions

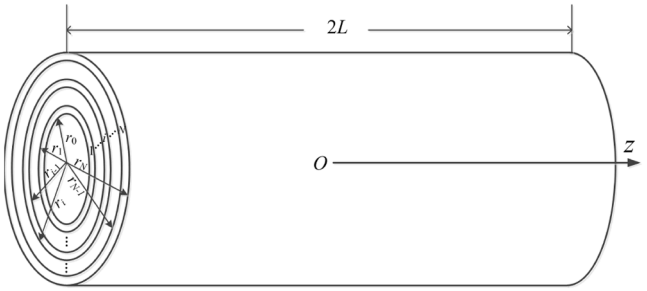

Fig. 1. A finite N-layered pipe of length $2L$.

$$u_\theta(r,z,0) = 0, \dot{u}_\theta(r,z,0) = 0 \tag{3}$$

and the boundary conditions

$$\sigma_1^{r\theta}\big|_{r=r_0} = \mu_1\left(\frac{\partial u_1^\theta}{\partial r} - \frac{u_1^\theta}{r}\right)\Big|_{r=r_0} = s_I(z,t),\ z \in [-L,\ L] \tag{4}$$

$$\sigma_N^{r\theta}\big|_{r=r_N} = \mu_N\left(\frac{\partial u_N^\theta}{\partial r} - \frac{u_N^\theta}{r}\right)\Big|_{r=r_N} = s_O(z,t),\ z \in [-L,\ L] \tag{5}$$

$$\sigma_i^{r\theta}\big|_{r=r_i} = \sigma_{i+1}^{r\theta}\big|_{r=r_i},\ i = 1,\ 2,\ \cdots,\ N-1,\ z \in [-L,\ L] \tag{6}$$

$$u_i^\theta\big|_{r=r_i} = u_{i+1}^\theta\big|_{r=r_i}, i = 1,\ 2,\ \cdots,\ N-1,\ z \in [-L,\ L] \tag{7}$$

$$\sigma_i^{z\theta}\big|_{z=\pm L} = \mu_i \frac{\partial u_i^\theta}{\partial z}\Big|_{z=\pm L} = 0, i = 1,\ 2,\ \cdots,\ N, r \in [r_0,\ r_N], \tag{8}$$

where $\sigma_i^{r\theta}$ and $\sigma_i^{z\theta}$ are two stress components corresponding to the ith layer, and s_I and s_O are the densities of the forces applied on its inner and outer surfaces, respectively.

3. Torsional vibration eigenfunctions

The eigenvalue problem corresponding to Eqs. (1)–(8) is formulated as

$$\mathbf{L}_i\left[u_i^\theta(r,z,t)\right] + \rho_i\omega^2 u_i^\theta(r,z,t) = 0, r \in [r_0,\ r_N], z \in [-L,\ L] \text{ in } \Omega_i \tag{9}$$

$$\mu_1\left(\frac{\partial u_1^\theta}{\partial r} - \frac{u_1^\theta}{r}\right)\Big|_{r=r_0} = 0, z \in [-L,\ L] \tag{10}$$

$$\mu_N\left(\frac{\partial u_N^\theta}{\partial r} - \frac{u_N^\theta}{r}\right)\Big|_{r=r_N} = 0, z \in [-L,\ L] \tag{11}$$

$$\sigma_i^{r\theta}\big|_{r=r_i} = \sigma_{(i+1)}^{r\theta}\big|_{r=r_i}, = 1,\ 2,\ \cdots,\ N-1, z \in [-L,\ L] \tag{12}$$

$$u_i^\theta\big|_{r=r_i} = u_{(i+1)}^\theta\big|_{r=r_i}, i = 1,\ 2,\ \cdots,\ N-1, z \in [-L,\ L] \tag{13}$$

$$\frac{\partial u_i^\theta}{\partial z}\Big|_{z=\pm L} = 0, i = 1,\ 2,\ \cdots,\ N,\ r \in [r_0,\ r_N] \tag{14}$$

Setting

$$u_\theta = R(r)Z(z) \tag{15}$$

then substituting Eq. (15) into Eq. (9), we have

$$Z''(z) + \xi^2 Z(z) = 0 \tag{16}$$

$$R''(r) + \frac{R'(r)}{r} + \left(\frac{\omega^2}{c_{iT}^2} - \xi^2 - \frac{1}{r^2}\right)R(r) = 0 \text{in } \Omega_i, \tag{17}$$

where ξ is the wave number, and

$$\mathrm{c_{iT}} = \sqrt{\frac{\mu_i}{\rho_i}}\mathrm{B} = [\mathrm{b_1}, \mathrm{b_2}, \ldots, \mathrm{b_M}]. \tag{18}$$

Solving Eq. (16) under the end boundary condition, i.e., Eq. (14), we obtain

$$(z) = A_k cos\xi_k z$$

where

$$\xi_k = \frac{k\pi}{L} \tag{19}$$

or

$$Z_k(z) = B_k sin\xi_k\ z\ \xi_k = \frac{(2k+1)\pi}{2L}. \tag{20}$$

where

Solving Eq. (17), we obtain

$$R_{ik}(r) = C_{ik}Z_1(\beta_{ik}r) + D_{ik}X_1(\beta_{ik}r)\ in\ \Omega_i,\ (i=1,\ 2,\ \ldots,\ N) \tag{21}$$

where

$$\beta_{ik}^2 = \eta_i\alpha_{ik}^2, \tag{22}$$

$$\alpha_{ik}^2 = \frac{\omega_k^2}{c_{iT}^2} - \xi_k^2, (i=1,\ 2,\ \cdots,\ N), \tag{23}$$

and

$$\eta_i = \begin{cases} 1,\ \alpha_{ik}^2 > 0 \\ -1,\ \alpha_{ik}^2 < 0 \end{cases}. \tag{24}$$

Z_1 and X_1 in Eq. (21) are the first order Bessel and Neumann functions, respectively, when $\eta_i = 1$. Z_1 and X_1 are the first order modified Bessel and Hankel functions, respectively, when $\eta_i = -1$. Substituting Eqs. (15) and (21) into Eqs. (10)-(13), we obtain a system of $2N$ homogeneous equations in the constants C_{ik} and D_{ik} (i = 1, 2, …, N). A necessary and sufficient condition for the existence of a solution is that the determinant of coefficients must be equal to zero, namely,

$$\left|d_{ij}\right|_{2N\times 2N} = 0, \tag{25}$$

where the expressions for d_{ij} are listed in Appendix A. Eq. (25) is the dispersion equation of the torsional guided wave propagation in the multilayered pipe. Solving Eq. (25), we obtain the values of ω_{mk} (m, k = 1, 2, 3, …) corresponding to each ξ_k.

In a word, the torsional vibration eigenfunctions can be formulated as

$$u_{imk}^{\theta}(r,z) = [C_{imk}Z_1(\beta_{imk}r) + D_{imk}X_1(\beta_{imk}r)]cos\xi_k z\ in\ \Omega_i,\ (i=1,\ 2,\ \ldots,\ N) \tag{26}$$

where $\xi_k = \frac{k\pi}{L}$, or

$$u_{imk}^{\theta}(r,z) = [C_{imk}Z_1(\beta_{imk}r) + D_{imk}X_1(\beta_{imk}r)]sin\xi_k z\ in\ \Omega_i,\ (i=1,\ 2,\ \ldots,\ N) \tag{27}$$

where $\xi_k = \frac{(2k+1)\pi}{2L}$.

4. Transient torsional wave propagation in the finite multilayered pipe

The solution to (1) under (3)–(8) can be expressed as

$$u_\theta(r,z,t) = u_\theta^a(r,z,t) + u_\theta^b(r,z,t) \tag{28}$$

where $u_\theta^a(r,z,t)$ is the solution to (1) under (3)–(8) with $s_I(z,t) = 0$ and $s_O(z,t) = 0$, and $u_\theta^b(r,z,t)$ is the solution to (1) under (3)–(8) with $f(r, z, t) = 0$. Thus, $u_\theta^a(r,z,t)$ is the transient response to the body force $f(r, z, t)$, whereas $u_\theta^b(r,z,t)$ is the transient response to the surface force $s_I(z,t)$ and $s_O(z,t)$. According to a similar derivation given by Reismann [36], Eringen and Suhubi [37], and Tang [33,34], we have

$$u_\theta^a(r,z,t) = \sum_{mk}\frac{1}{M_{mk}\omega_{mk}}\left[\int_0^t Q_{mk}^a(\tau)sin\omega_{mk}(t-\tau)d\tau\right]u_{mk}^{\theta}(r,z), \tag{29}$$

where

$$Q_{mk}^a(t) = \sum_{i=1}^{N}\int_{\Omega_i}\rho_i u_{imk}^{\theta}(r,z)f_i(r,z,t)dV, \tag{30}$$

and

$$M_{mk} = 2\pi\sum_{i=1}^{N}\int_{-L}^{L}\int_{r_0}^{r_N}\rho_i\left|u_{imk}^{\theta}(r,z)\right|^2 rdrdz. \tag{31}$$

Eqs. (29)–(31) represent the exact transient torsional response of the multilayered pipe to the body force. It is difficult to obtain the exact analytical expression of $u_\theta^b(r,z,t)$. According to the method presented in Ref. [34], the approximate expression of $u_\theta^b(r,z,t)$ can be obtained, and it is formulated as

$$u_\theta^b(r,z,t) = \sum_{mk}\frac{1}{M_{mk}\omega_{mk}}\left[\int_0^t Q_{mk}^b(\tau)sin\omega_{mk}(t-\tau)d\tau\right]u_{mk}^{\theta}(r,z), \tag{32}$$

where

$Q_{mk}^b(t) = \int_{\Sigma_I} u_{1mk}^{\theta}(r,z)s_I(z,t)dS + \int_{\Sigma_O} u_{Nmk}^{\theta}(r,z)s_O(z,t)dS$. (33).

Eqs. (28), (29) and (32) represent the analytical transient torsional response of the finite multilayered pipe to external body and surface forces.

5. Transient torsional wave propagation in the infinite multilayered pipe

Substituting Eq. (26) or (27) into Eq. (31), we have

$$M_{mk} = LM_{mk}^{\infty}, \tag{34}$$

where

$$M_{mk}^{\infty} = \sum_{i=1}^{N}\int_{r_0}^{r_N}\rho_i[C_{imk}Z_1(\beta_{imk}r) + D_{imk}X_1(\beta_{imk}r)]^2 rdr. \tag{35}$$

From Eqs. (19) and (20), we know that the interval between two successive wave numbers is

$$\Delta\xi_k = \frac{\pi}{L}. \tag{36}$$

Substitution of Eq. (36) into Eq. (34) gives

$$M_{mk} = \frac{\pi}{\Delta\xi_k}M_{mk}^{\infty}. \tag{37}$$

Substituting Eq. (37) into Eqs. (29) and (32) and using Eq. (28), we have

$$u_\theta(r,z,t) = \sum_{mk}\frac{1}{\pi M_{mk}^{\infty}\omega_{mk}}\left[\int_0^t Q_{mk}(\tau)sin\omega_{mk}(t-\tau)d\tau\right]u_{mk}^{\theta}(r,z)\Delta\xi_k, \tag{38}$$

where

$$Q_{mk}(t) = \sum_{i=1}^{N}\int_{\Omega_i}\rho_i u_{imk}^{\theta}(r,z)f_i(r,z,t)dV + \int_{\Sigma_I}u_{1mk}^{\theta}(r,z)s_I(z,t)dS + \int_{\Sigma_O}u_{Nmk}^{\theta}(r,z)s_O(z,t)dS. \tag{39}$$

If the multilayered pipe is of infinite length, i.e., $L \to \infty$, the interval between two successive wave numbers $\Delta\xi_k$ approaches zero. Therefore, the summation over the index k in (38) will be replaced by the integral over the continuous wave numbers ξ. We have

$$u_\theta(r,z,t) = \sum_m\int_0^{\infty}\frac{1}{\pi M_m^{\infty}\omega_m}\left[\int_0^t Q_m(\tau)sin\omega_m(t-\tau)d\tau\right]u_m^{\theta}(r,z)d\xi. \tag{40}$$

Eq. (40) represents the analytical transient torsional response of the infinite multilayered pipe.

6. Numerical examples

In this section, the excitation and propagation of transient torsional wave in a finite bi-layered pipe, as shown in Fig. 2, is numerically studied as an example. The length of the pipe is 0.6 m; r_0, r_1 and r_2 are 0.03 m, 0.035 m and 0.04 m, respectively. The inner pipe is made of aluminum (Al). Its density is $\rho_1 = 2.7 \times 10^3$ kg/m^3 and Lamé's second constant is $u_1 = 2.5 \times 10^{10}$ kg/m^3. The outer pipe is made of copper (Cu). Its density is $\rho_2 = 8.9 \times 10^3$ kg/m^3 and Lamé's second constant is $\mu_2 = 3.9 \times 10^{10}$ kg/m^3.

6.1. Dispersion analysis

The dispersion equation corresponding to torsional waves propagating in the bi-layered pipe can be obtained from Eq. (25) by setting $N = 2$. Dispersion curves can be obtained by solving the dispersion equation. Figs. 3(a) and (b) show the phase and group velocity dispersion curves corresponding to torsional waves in pipes, respectively. The blue dash dot lines, red dash lines and black solid lines are corresponding to torsional waves in the Al pipe, Cu pipe, and Al-Cu bi-layered pipe, respectively. It is noted that the Al or Cu pipe has the same inner and outer radius with the Al-Cu bi-layered pipe in the following discussion.

The first torsional wave mode T(0, 1) in a homogeneous pipe is nondispersive across the whole frequency range, as shown in Fig. 3. However, this mode in a bi-layered pipe is dispersive. Fig. 3 shows that T (0, 1) mode has weak dispersion when the frequency is below 200 kHz, and it seems to be nondispersive when the frequency is greater than 200 kHz. It is assumed that c_{pmk}^{Al}, c_{pmk}^{Cu} and c_{pmk}^{Bi} are the phase velocities of the mth order torsional mode at a given frequency f_k in the Al, Cu and Al-Cu bi-layered pipes, respectively. Fig. 3(a) shows that $c_{pmk}^{\mathrm{Cu}} < c_{pmk}^{\mathrm{Bi}} < c_{pmk}^{\mathrm{Al}}$. Fig. 3(b) shows that the group velocity of T(0, m) ($m = 2, 3, 4, \ldots$) modes is lower than that of T(0, 1) mode if the pipe is homogeneous. However, the group velocity of T(0, m) ($m = 3, 4, 5, \ldots$) modes may be greater than that of T(0, 1) mode if the pipe is bi-layered. For example, T(0, 3) mode around 400 kHz and T(0, 4) mode around 700 kHz have a greater group velocity than T(0, 1) mode, as shown in Fig. 3(b).

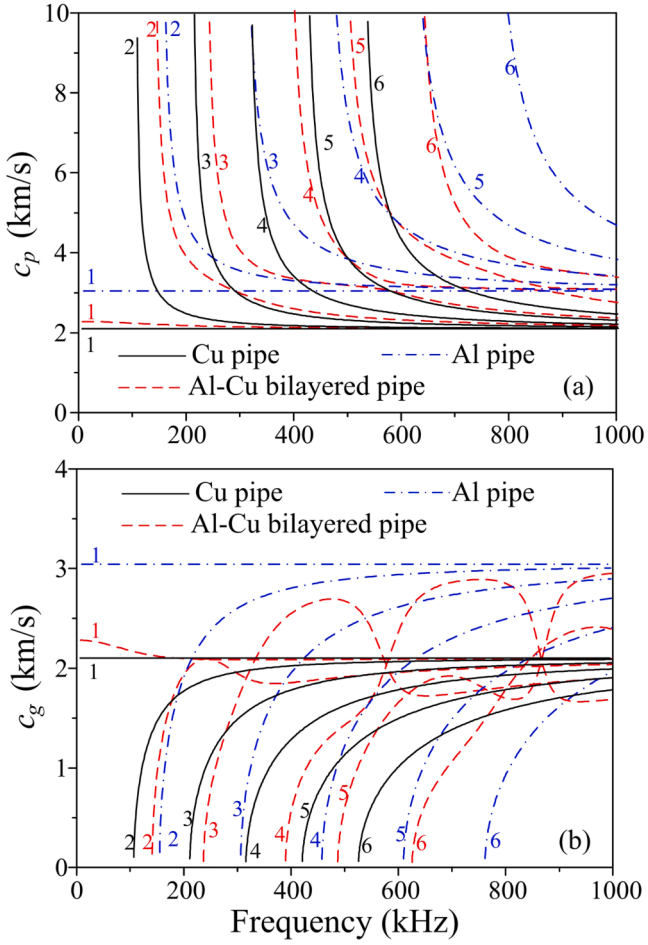

Fig. 3. The phase and group velocity dispersion curves of the first sixth order torsional waves in the Cu pipe, Al pipe and Al-Cu bilayered pipe. (a) Phase velocity dispersion curves; (b) Group velocity dispersion curves.

6.2. Displacement distribution

Fig. 4 shows the eigendisplacement amplitude $R_{mk}(r)$ corresponding to the first six modes as a function of r/r_2 when ξh=6.1785, where

$$R_{mk}(r) = \begin{cases} C_{1mk}Z_1(\beta_{1mk}r) + D_{1mk}X_1(\beta_{1mk}r) \ in\ \Omega_1 \\ C_{1mk}Z_1(\beta_{2mk}r) + D_{1mk}X_1(\beta_{2mk}r) \ in\ \Omega_2 \end{cases}. \tag{41}$$

The eigendisplacement amplitude of T(0, 1)mode, i.e., $R_{1k}(r)$ increases with an increase in r/r_2, as shown in Fig. 4(a). The eigendisplacement distribution as a function of r/r_2 in the inner Al pipe is distinct from that in the outer Cu pipe for higher order torsional modes, as shown in Figs. 4(b)-4(f). The variation of r has a strong influence on the eigendisplacement of T(0, 2) mode in the outer Cu pipe. However, it has a weak influence on that of the inner Al pipe, as shown in Fig. 4(b). It seems that the eigendisplacement in the outer Cu pipe is a cosine function of r/r_2, and there are $m/4$ cycles, where m is the order of the mode. The eigendisplacement in the inner Al pipe also seems like a cosine function of r/r_2. However, it has different cycles from that of the outer Cu pipe.

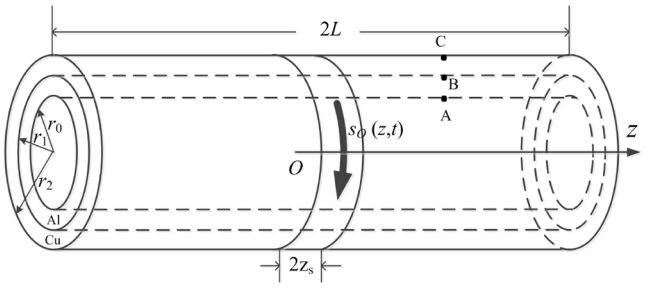

Fig. 2. An Al-Cu bilyaered pipe of length 2L. The inner and outer radius of the inner Al pipe are r_0 and r_1, respectively. The inner and outer radius of the outer Cu pipe are r_1 and r_2, respectively. The torsional surface force applied on the outer surface is s_O(z, t) where -z_s < z < z_s. Receiving points A, B and C are located on the inner surface, interface and outer surface, respectively.

6.3. Transient torsional waves excited by a surface force in the finite Al-Cu bi-layered pipes

The axisymmetric torsional surface force is applied on the outer surface of the finite bi-layered Al-Cu pipe, as shown in Fig. 2. A narrow band signal consisting of eight cycles is used as the exciting signal. Thus, s_O (z, t) shown in Fig. 2 can be formulated as

$$s_O(z,t) = T_0 \sin(2\pi f_0 t)\left[0.5 - 0.5\cos\left(\frac{2\pi t}{8/f_0}\right)\right],\ z \in [-z_s,\ +z_s]. \tag{42}$$

In the following calculation, the excitation center frequency f_0 is chosen as 180 kHz,z_s is set to 4 mm, and T_0 is set to 10^8. It can be found from Fig. 3(b) that only T(0,1) and T(0, 2) modes can be excited by this surface force, whose frequency range is about 135 kHz ~ 225 kHz. Substituting Eq. (42) into Eqs. (32) and (33), we can obtain the transient displacement corresponding to each torsional mode. Moreover, the total transient displacement can be obtained from the superposition of all modes excited.

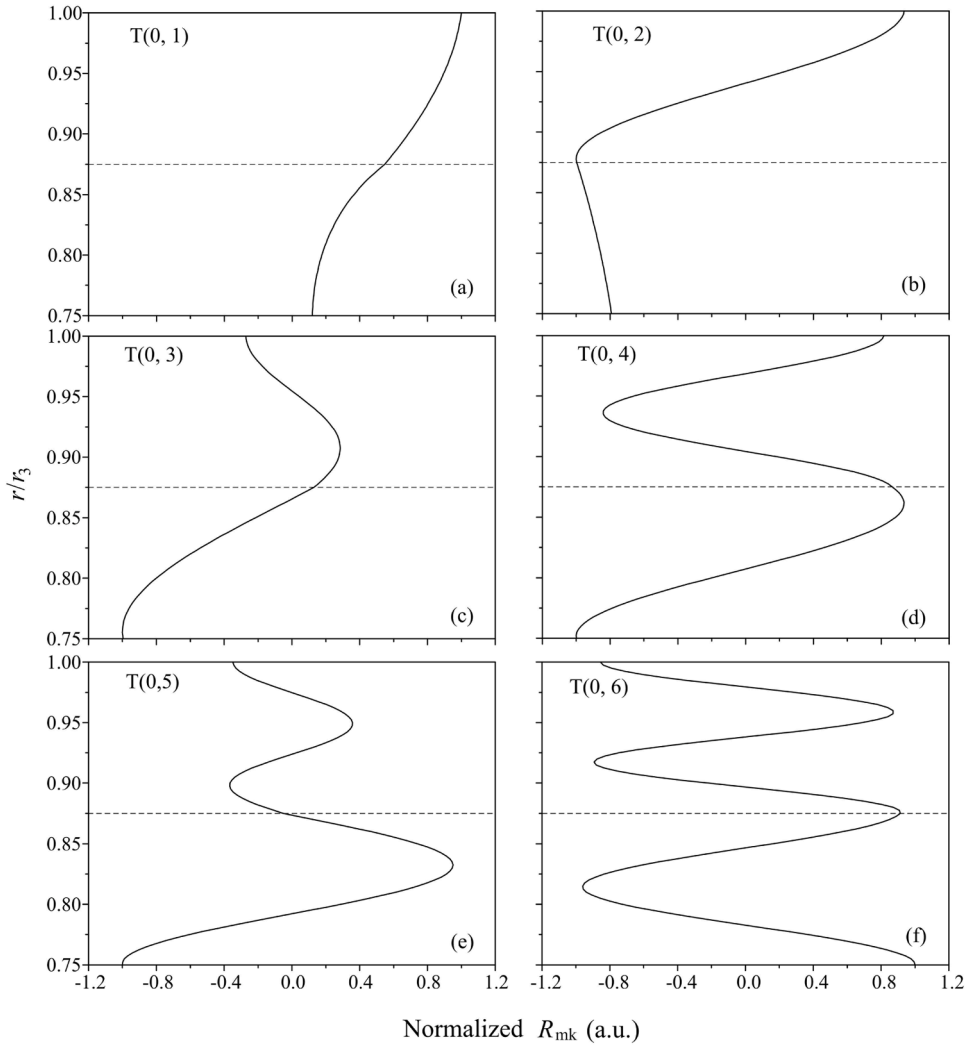

Fig. 4. Eigendisplacement amplitude $R_{mk}(r)$ corresponding to the first sixth modes as a function of r/r_2 when ξh=6.1785. (a) T(0, 1); (a) T(0, 2); (a) T(0, 3); (a) T(0, 4); (a) T(0, 5); (a) T(0, 6).

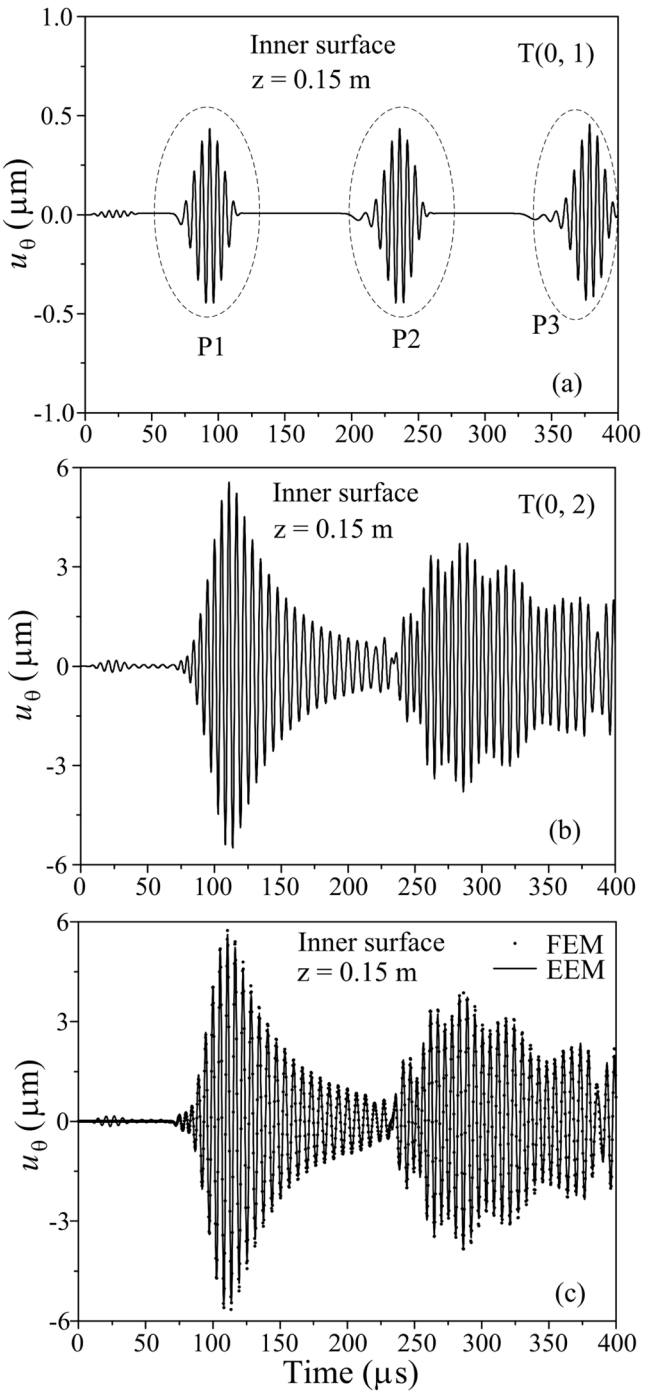

Fig. 5. The transient displacements of T(0, 1) (a) and T(0, 2) (b) modes, and the total transient displacement (c) received at the point A on the inner surface of the Al-Cu bilayered pipe. The solid and dot lines in (c) are computed by eigenfunction expansion method (EEM) and finite element method (FEM), respectively. The external axisymmetric torsional force is applied on the outer surface of the pipe, and the width of the force is $2z_s$. The distance between the center of the force and the receiving point is 0. 15 m.

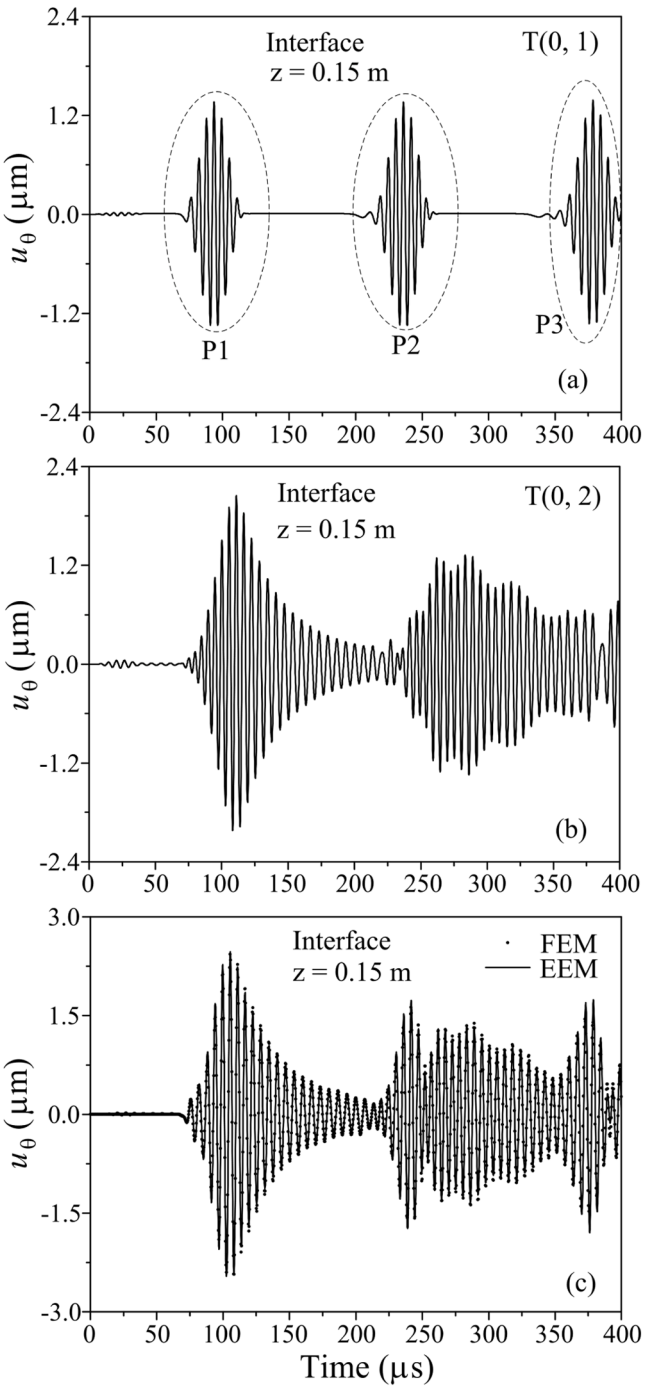

Fig. 6. The transient displacements of T(0, 1) (a) and T(0, 2) (b) modes, and the total transient displacement (c) received at the point B on the interface of the Al-Cu bilayered pipe. The solid and dot lines in (c) are computed by eigenfunction expansion method (EEM) and finite element method (FEM), respectively. The external axisymmetric torsional force is applied on the outer surface of the pipe, and the width of the force is $2z_s$. The distance between the center of the force and the receiving point is 0. 15 m.

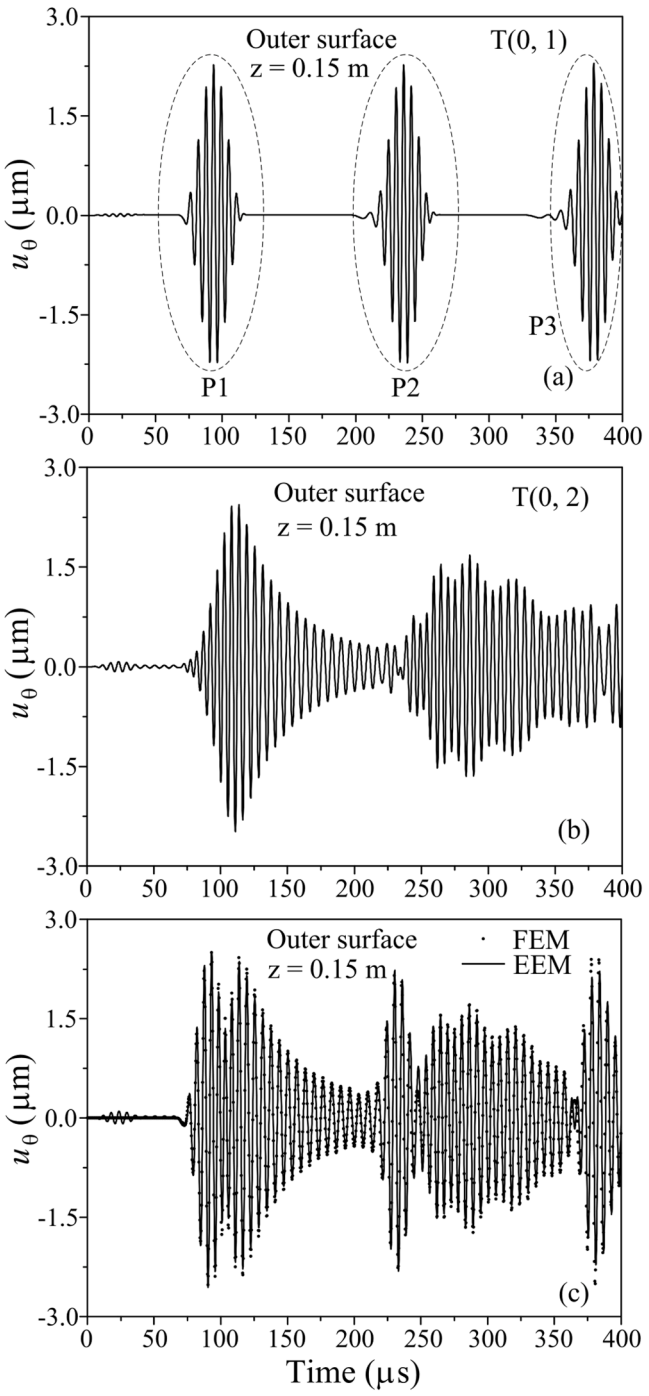

Fig. 7. The transient displacements of T(0, 1) (a) and T(0, 2) (b) modes, and the total transient displacement (c) received at the point C on the outer surface of the Al-Cu bilayered pipe. The solid and dot lines in (c) are computed by eigenfunction expansion method (EEM) and finite element method (FEM), respectively. The external axisymmetric torsional force is applied on the outer surface of the pipe, and the width of the force is $2z_s$. The distance between the center of the force and the receiving point is 0. 15 m.

The receiving points A, B and C are located on the inner surface, interface and outer surface of the Al-Cu bi-layered pipe, respectively, as shown in Fig. 2. The axial distance between the center of the surface force and the receiving points is 0.15 m. Figs. 5(a) and (b) show the transient torsional displacements of T(0, 1) and T(0, 2) received at point A on the inner surface, respectively. Fig. 3 shows that T(0, 1) mode has a very weak dispersion; however, mode T(0, 2) has a strong dispersion around 180 kHz. Therefore, it seems that the waveform of T(0, 1) mode has no distortion during the propagation, as shown in Fig. 5(a). However, the waveform of T(0, 2) mode has great distortion, as shown in Fig. 5(b). The wave package P1 in Fig. 5(a) is directly received. The wave packages P2 and P3 are reflected from the right and left boundaries, respectively. Furthermore, comparing Fig. 5(b) with Fig. 5(a), we know that the mode T(0, 2) is the dominant mode in the transient torsional displacement, received from the point located on the inner surface of the Al-Cu bi-layered pipe. This agrees with the result shown in Figs. 4(a) and 4(b). The solid line in Fig. 5(c) is the total transient torsional displacement, which is obtained from the superposition of T(0, 1) mode in Fig. 5(a) and T(0, 2) mode in Fig. 5(b). The point line in Fig. 5 (c) is obtained by the FEM.

Figs. 6(a) and 6(b) show the transient torsional displacements of T(0, 1) and T(0, 2) at point B on the interface of the Al-Cu bi-layered pipe obtained using the EEM, respectively. Figs. 7(a) and 7(b) show those of T (0, 1) and T(0, 2) at point C on the outer surface of the bi-layered pipe obtained using the EEM, respectively. The solid lines in Figs. 6(c) and 7 (c) are the total transient torsional displacement at points B and C obtained using the EEM, respectively. They are obtained from the superposition of T(0, 1) and T(0, 2) modes. The point lines in Figs. 6(c) and 7 (c) are the transient torsional displacement at points B and C obtained using the FEM, respectively. Figs. 6(c) and 7(c) show that the results obtained by the EEM and FEM agree very well.

In the FEM simulation, the commercial finite element software called Abaqus is used. Eight-node solid elements are employed. The element size along the z-axis is 0.3 mm. There are 30 and 600 elements along the r and θ axes, respectively. The time-step is 0.02 μs in the explicit algorithm. It is found that the results obtained by the EEM and FEM agree very well. On our Intel Xeon E5-2620×2 workstation, to produce the results shown in Figs. 5(c), 6(c) and 7(c), the FEM took about five hours, and the EEM took less than two minutes. In addition, 24 threads were employed in the FEM simulation, whereas only one thread was used by the EEM. Therefore, compared with the FEM simulation, the solution obtained using the EEM can be numerically evaluated with a higher computational efficiency.

7. Conclusions

In this study, the excitation and propagation of transient torsional guided waves in a multilayered pipe is investigated. The analytical solution of the elastodynamic response of the finite and infinite multilayered pipes to body forces is derived by the EEM. Moreover, the approximate analytical solution of the elastodynamic response of these pipes to surface forces is obtained. The form of the solution presented here is concise. Compared with the FEM, the theory presented here has two main advantages. Firstly, the influence of external forces on the excitation of each torsional guided wave mode can be quantitatively analyzed. It is very important in the determination of the mode and frequency band used to inspect the pipe. Secondly, the solution obtained using the EEM can be numerically evaluated with high computational efficiency. Therefore, the theory presented here is far more efficient than the FEM when simulating the torsional wave propagation in multilayered pipe. In practice, the solution obtained using the EEM can be used to determine the mode and frequency band for the pipe inspection. The FEM can be used to study the interaction between the guided wave and the defects in pipes.

CRediT authorship contribution statement

Chuanwen Chen: Writing – original draft, Investigation, Writing – review & editing. **Yang Xiang:** Investigation, Data curation, Writing – review & editing. **Lei Qin:** Software, Formal analysis. **Liguo Tang:** Writing – review & editing, Methodology, Conceptualization. **Wenyu Luo:** Validation, Writing – review & editing.

Declaration of competing interest

The authors declare that they have no known competing financial interests or personal relationships that could have appeared to influence the work reported in this paper.

Acknowledgements

This work was supported by the National Natural Science Foundation of China (Grant No. 12274358), Guangdong Basic and Applied Basic Research Foundation (Grant No. 2024A1515010019), State Key laboratory of Acoustics, Chinese Academy of Science (Grant No. SKLA202309), Qin Xin Talents Cultivation Program, Beijing Information Science & Technology University (QXTCP A202103), and the open research fund of Key Laboratory of Sensors, Beijing Information Science and Technology University.

Appendix A

The formulation of d_{ij} in Eq. 25 is as follows:

$$d_{11} = \mu_1\beta_1\left[V_1{}'(\beta_1 r_0) - \frac{1}{\beta_1 r_0}V_1(\beta_1 r_0)\right] \tag{A.1}$$

$$d_{12} = \mu_1\beta_1\left[W_1{}'(\beta_1 r_0) - \frac{1}{\beta_1 r_0}W_1(\beta_1 r_0)\right] \tag{A.2}$$

$$d_{13} = \cdots = d_{1(2N)} = 0 \tag{A.3}$$

$$d_{21} = V_1(\beta_1 r_1) \tag{A.4}$$

$$d_{22} = W_1(\beta_1 r_1) \tag{A.5}$$

$$d_{23} = -V_1(\beta_2 r_1) \tag{A.6}$$

$$d_{24} = -W_1(\beta_2 r_1) \tag{A.7}$$

$$d_{25} = \cdots = d_{2(2N)} = 0 \tag{A.8}$$

$$d_{31} = \mu_1\beta_1\left[V_1{}'(\beta_1 r_1) - \frac{1}{\beta_1 r_1}V_1(\beta_1 r_1)\right] \tag{A.9}$$

$$d_{32} = \mu_1\beta_1\left[W_1{}'(\beta_1 r_1) - \frac{1}{\beta_1 r_1}W_1(\beta_1 r_1)\right] \tag{A.10}$$

$$d_{33} = -\mu_2\beta_2\left[V_1{}'(\beta_2 r_1) - \frac{1}{\beta_2 r_1}V_1(\beta_2 r_1)\right] \tag{A.11}$$

$$d_{34} = -\mu_2\beta_2\left[W_1{}'(\beta_2 r_1) - \frac{1}{\beta_2 r_1}W_1(\beta_2 r_1)\right] \tag{A.12}$$

$$d_{35} = \cdots = d_{3(2N)} = 0 \tag{A.13}$$

...

$$d_{(2i)1} = \cdots = d_{(2i)(2i-2)} = 0 \tag{A.14}$$

$$d_{(2i)(2i-1)} = V_1(\beta_i r_i) \tag{A.15}$$

$$d_{(2i)(2i)} = W_1(\beta_i r_i) \tag{A.16}$$

$$d_{(2i)(2i+1)} = -V_1(\beta_{i+1} r_i) \tag{A.17}$$

$$d_{(2i)(2i+2)} = -W_1(\beta_{i+1} r_i) \tag{A.18}$$

$$d_{(2i)(2i+3)} = \cdots = d_{(2i)(2N)} = 0 \tag{A.19}$$

$$d_{(2i+1)1} = \cdots = d_{(2i+1)(2i-2)} = 0 \tag{A.20}$$

$$d_{(2i+1)(2i-1)} = \mu_i\beta_i\left[V_1{}'(\beta_i r_i) - \frac{1}{\beta_i r_i}V_1(\beta_i r_i)\right] \tag{A.21}$$

$$d_{(2i+1)(2i)} = \mu_i\beta_i\left[W_1{}'(\beta_i r_i) - \frac{1}{\beta_i r_i}W_1(\beta_i r_i)\right] \tag{A.22}$$

$$d_{(2i+1)(2i+1)} = -\mu_{i+1}\beta_{i+1}\left[V_1{}'(\beta_{i+1} r_i) - \frac{1}{\beta_{i+1} r_i}V_1(\beta_{i+1} r_i)\right] \tag{A.23}$$

$$d_{(2i+1)(2i+2)} = -\mu_{i+1}\beta_{i+1}\left[W_1{}'(\beta_{i+1}r_i) - \frac{1}{\beta_{i+1}r_i}W_1(\beta_{i+1}r_i)\right] \tag{A.24}$$

$$d_{(2i+1)(2i+3)} = \cdots = d_{(2i+1)(2N)} = 0 \tag{A.25}$$

$$(i = 2,\ 3,\ \ldots,\ N-2)d_{(2N-2)1} = \cdots = d_{(2N-2)(2N-4)} = 0 \tag{A.26}$$

$$d_{(2N-2)(2N-3)} = V_1(\beta_{N-1}r_{N-1}) \tag{A.27}$$

$$d_{(2N-2)(2N-2)} = W_1(\beta_{N-1}r_{N-1}) \tag{A.28}$$

$$d_{(2N-2)(2N-1)} = -V_1(\beta_N r_{N-1}) \tag{A.29}$$

$$d_{(2N-2)(2N)} = -W_1(\beta_N r_{N-1}) \tag{A.30}$$

$$d_{(2N-1)1} = \cdots = d_{(2N-1)(2N-4)} = 0 \tag{A.31}$$

$$d_{(2N-1)(2N-3)} = \mu_{N-1}\beta_{N-1}\left[V_1{}'(\beta_{N-1}r_{N-1}) - \frac{1}{\beta_{N-1}r_{N-1}}V_1(\beta_{N-1}r_{N-1})\right] \tag{A.32}$$

$$d_{(2N-1)(2N-2)} = \mu_{N-1}\beta_{N-1}\left[W_1{}'(\beta_{N-1}r_{N-1}) - \frac{1}{\beta_{N-1}r_{N-1}}W_1(\beta_{N-1}r_{N-1})\right] \tag{A.33}$$

$$d_{(2N-1)(2N-1)} = -\mu_N\beta_N\left[V_1{}'(\beta_N r_{N-1}) - \frac{1}{\beta_N r_{N-1}}V_1(\beta_N r_{N-1})\right] \tag{A.34}$$

$$d_{(2N-1)(2N)} = -\mu_N\beta_N\left[W_1{}'(\beta_N r_{N-1}) - \frac{1}{\beta_N r_{N-1}}W_1(\beta_N r_{N-1})\right] \tag{A.35}$$

$$d_{(2N)1} = \cdots = d_{(2N)(2N-2)} = 0 \tag{A.36}$$

$$d_{(2N)(2N-1)} = \mu_N\beta_N\left[V_1{}'(\beta_N r_N) - \frac{1}{\beta_N r_N}V_1(\beta_N r_N)\right] \tag{A.37}$$

$$d_{(2N)(2N)} = \mu_N\beta_N\left[W_1{}'(\beta_N r_N) - \frac{1}{\beta_N r_N}W_1(\beta_N r_N)\right] \tag{A.38}$$

where

$$\beta_i^2 = \eta_i\alpha_i^2, (i=1,\ 2,\ \cdots,\ N) \tag{A.39}$$

$$\alpha_i^2 = \frac{\omega^2}{c_{iT}^2} - \xi^2, \tag{A.40}$$

$$\eta_i = \begin{cases} 1, & \alpha_i^2 > 0 \\ -1, & \alpha_i^2 < 0 \end{cases}. \tag{A.41}$$

V_1 and W_1 in Eqs. (A.1)-(A.38) are the first order Bessel and Neumann functions, respectively, when $\eta_i = 1$. V_1 and W_1 are the first order modified Bessel and Hankel functions, respectively, when $\eta_i = -1$.

Data availability

Data will be made available on request.

References

[1] A. Amiri, A. Masoumi, R. Talebitooti, Flutter and bifurcation instability analysis of fluid-conveying micro-pipes sandwiched by magnetostrictive smart layers under thermal and magnetic field, Int. J. Mech. Mater. Des. 16 (2020) 569–588, https://doi.org/10.1007/s10999-020-09487-w.

[2] J. Gao, Y. Lyu, M. Zheng, M. Liu, H. Liu, B. Wu, C. He, Application of state vector formalism and Legendre polynomial hybrid method in the longitudinal guided wave propagation analysis of composite multi-layered pipes, Wave Motion 100 (2021) 102670, https://doi.org/10.1016/j.wavemoti.2020.102670.

[3] Y. Zhang, B. Li, F. Tian, L. Xu, Propagation characteristic of axial and circumferential interface waves and detection of the interlaminar defect in multilayered pipes, Meas. Sci. Technol. 32 (2021), https://doi.org/10.1088/1361-6501/abb868, 025601 025601.

[4] R. Hashemian, M. Mohareb, Buckling finite element formulation for sandwich pipes under external pressure, Int. J. Pres. Ves. Pip. 147 (2016) 41–54, https://doi.org/10.1016/j.ijpvp.2016.09.006.

[5] R. Sburlati, M. Kashtalyan, Elasticity analysis of sandwich pipes with functionally graded interlayers, Eur. J. Mech. A-solid. 59 (2016) 232–241, https://doi.org/10.1016/j.euromechsol.2016.03.012.

[6] F.H. Quintanilla, M.J.S. Lowe, R.V. Craster, The symmetry and coupling properties of solutions in general anisotropic multilayer waveguides, J. Acoust. Soc. Am. 141 (2017) 406–418, https://doi.org/10.1121/1.4973543.

[7] D.N. Alleyne, B. Pavlakovic, M.J.S. Lowe, P. Cawley, Rapid long-range inspection of chemical plant pipework using guided waves, Insight 43 (2001) 93–96, https://doi.org/10.1063/1.1373757.

[8] H. Jia, M. Jing, L.R. Joseph, Guided wave propagation in single and double layer hollow cylinders embedded in infinite media, J. Acoust. Soc. Am. 129 (2011) 691–700, https://doi.org/10.1121/1.3531807.

[9] W. Luo, J.L. Rose, Phased array focusing with guided waves in a viscoelastic coated hollow cylinder, J. Acoust. Soc. Am. 121 (2007) 1945–1955, https://doi.org/10.1121/1.2711145.

[10] R.M. Sanderson, P.P. Catton, The reflection of guided waves from multiple flaws in pipes, J. Nondestruct. Eval. 32 (2013) 384–397, https://doi.org/10.1007/s10921-013-0192-x.

[11] Y. Zhang, B. Li, J. Wang, Periodical focusing phenomenon of ultrasonic guided waves in pipes, IEEE. T. Ultrason. Ferr. 69 (2022) 359–368, https://doi.org/10.1109/tuffc.2021.3110523.

[12] M. Pourmansouri, R. Mosalmani, A. Yaghootian, A. Ghanbarzadeh, Detecting and locating delamination defect in multilayer pipes using torsional guided wave, Arch. Appl. Mech. 92 (2022) 1037–1052, https://doi.org/10.1007/s00419-021-02091-0.
[13] Z. Fan, X. Niu, B. Miao, H. Meng, Hybrid coded excitation of the torsional guided wave mode T(0,1) for oil and gas pipeline inspection, Appl. Sci.-Basel 12 (2022) 777, https://doi.org/10.3390/app12020777.
[14] R. Praetzel, T. Clarke, D. Schmidt, H. de Oliveira, W.C. Dias da Silva, Monitoring the evolution of localized corrosion damage under composite repairs in pipes with guided waves, Ndt&e. Int. 122 (2021), https://doi.org/10.1016/j.ndteint.2021.102477, 102477 102477.
[15] D.C. Gazis, Three-dimensional investigation of the propagation of waves in hollow circular cylinders, J. Acoust. Soc. Am. 31 (1959) 568–573, https://doi.org/10.1121/1.1907753.
[16] A.H. Meitzler, Mode coupling occurring in the propagation of elastic pulses in wires, J. Acoust. Soc. Am. 33 (1961) 435–445, https://doi.org/10.1121/1.1908685.
[17] J. Zemanek, An experimental and theoretical investigation of elastic wave propagation in a cylinder, J. Acoust. Soc. Am. 51 (1971) 265–283, https://doi.org/10.1121/1.1912838.
[18] F. Karpfinger, B. Gurevich, H.-P. Valero, A. Bakulin, B. Sinha, Tube wave signatures in cylindrically layered poroelastic media computed with spectral method, Geophys. J. Int. 183 (2010) 1005–1013, https://doi.org/10.1111/j.1365-246X.2010.04773.x.
[19] L.L. Aguiar, C.A. Almeida, G.H. Paulino, Dynamic analysis of risers using a novel multilayered pipe beam element model, Mar. Struct. 44 (2015) 211–231, j.marstruc.2015.08.004.
[20] S. Banerjee, T. Kundu, Elastic wave field computation in multilayered nonplanar solid structures: a mesh-free semianalytical approach, J. Acoust. Soc. Am. 123 (2008) 1371–1382, https://doi.org/10.1121/1.2823258.
[21] M.V. Predoi, Guided waves dispersion equations for orthotropic multilayered pipes solved using standard finite elements code, Ultrasonics 54 (2014) 1825–1831, https://doi.org/10.1016/j.ultras.2014.01.019.
[22] J.N. Barshinger, J.L. Rose, Guided wave propagation in an elastic hollow cylinder coated with a viscoelastic material, IEEE. T. Ultrason. Ferr. 51 (2004) 1547–1556, https://doi.org/10.1109/tuffc.2004.1367496.
[23] D.N. Alleyne, P. Cawley, Long range propagation of Lamb waves in chemical plant pipework, Mater. Eval. 55 (1997) 504–508, https://doi.org/10.1016/S1044-5803(97)00084-3.
[24] D.N. Alleyne, P. Cawley, The interaction of Lamb waves with defects, IEEE T. Ultrason. Ferr. 39 (1992) 381–397, https://doi.org/10.1016/S0963-8695(96)80275-1.
[25] A. Demma, P. Cawley, M. Lowe, A.G. Roosenbrand, The reflection of the fundamental torsional mode from cracks and notches in pipes, J. Acoust. Soc. Am. 114 (2003) 611–625, https://doi.org/10.1121/1.1582439.
[26] A. Demma, P. Cawley, M. Lowe, A.G. Roosenbrand, B. Pavlakovic, The reflection of guided waves from notches in pipes: a guide for interpreting corrosion measurements, Ndt&e. Int. 37 (2004) 167–180, https://doi.org/10.1016/j.ndteint.2003.09.004.
[27] J. Ma, F. Simonetti, M.J.S. Lowe, Scattering of the fundamental torsional mode by an axisymmetric layer inside a pipe, J. Acoust. Soc. Am. 120 (2006) 1871–1880, https://doi.org/10.1121/1.2336750.
[28] J. Ma, M.J.S. Lowe, F. Simonetti, Feasibility study of sludge and blockage detection inside pipes using guided torsional waves, Meas. Sci. Technol. 18 (2007) 2629–2641, https://doi.org/10.1088/0957-0233/18/8/039.
[29] W. Duan, J. Kanfoud, M. Deere, P. Mudge, T.-H. Gan, Spectral subtraction and enhancement for torsional waves propagating in coated pipes, Ndt&e. Int. 100 (2018) 55–63, https://doi.org/10.1016/j.ndteint.2018.08.009.
[30] M. Ratassepp, S. Fletcher, M.J.S. Lowe, Scattering of the fundamental torsional mode at an axial crack in a pipe, J. Acoust. Soc. Am. 127 (2010) 730–740, https://doi.org/10.1121/1.3277185.
[31] H.W. Kim, Y.E. Kwon, J.K. Lee, Y.Y. Kim, Higher torsional mode suppression in a pipe for enhancing the first torsional mode by using magnetostrictive patch transducers, IEEE. T. Ultrason. Ferr. 60 (2013) 562–572, https://doi.org/10.1109/tuffc.2013.2597.
[32] L.G. Tang, X.M. Xu, Transient torsional vibration responses of finite, semi-infinite and infinite hollow cylinders, J. Sound Vib. 329 (2010) 1089–1100, https://doi.org/10.1016/j.jsv.2009.10.031.
[33] L. Tang, Z. Wu, Elastodynamic response of bonded solids using the method of eigenfunction expansion, J. Eng. Math. 74 (2012) 101–118, https://doi.org/10.1007/s10665-011-9488-y.
[34] L. Tang, Z. Wu, S. Liu, W. Yang, Three-dimensional analytical solution for transient guided wave propagation in liquid-filled pipe systems, IEEE. T. Ultrason. Ferr. 59 (2012) 1759–1773, https://doi.org/10.1109/tuffc.2012.2380.
[35] X.C. Yin, Z.Q. Yue, Transient plane-strain response of multilayered elastic cylinders to axisymmetric impulse, J. Appl. Mech-t. Asme. 69 (2002) 825–835, https://doi.org/10.1115/1.1505625.
[36] H. Reismann, On the forced motion of elastic solids, Appl. Sci. Res. 18 (1967) 156–165, https://doi.org/10.1007/BF00382343.
[37] A.C. Eringen, E.S. Suhubi, Elastodynamics, Academic, New York, 1975.